Article | Received 17 September 2025; Revised 5 December 2025; Accepted 9 December 2025; Published 12 January 2026
https://doi.org/10.55092/am20260001

Casting of complex open cellular structures using high manganese steel

Claudia Drebenstedt[1,*], Jörg Hohlfeld[1], Christian Hannemann[1], Nadja Berndt[1], Ulrich Krupp[2], Thomas Hipke[1], Dilay Kibaroglu[3] and Christian Haase[3]

[1] Fraunhofer Institute for Machine Tools and Forming Technology IWU, 09126 Chemnitz, Germany
[2] RWTH Aachen University, Steel Institute, 52072 Aachen, Germany
[3] Technical University Berlin, Chair Materials for Additive Manufacturing, 10587 Berlin, Germany

* Correspondence author; E-mail: claudia.drebenstedt@iwu.fraunhofer.de.

Highlights:

- Design of a special periodic open cellular lattice structure.
- Investment casting of high manganese steel with different amounts of aluminum for using TRIP/TWIP-effects.
- Comparison of energy absorption levels.

Abstract: High manganese steels offer an excellent combination of high strength and good ductility, making them ideal for lightweight and energy absorbing applications such as open cellular structures. Additive manufacturing is often used to produce metallic open cellular structures since it allows a high complexity of the geometry and high material efficiency, but the structures often exhibit anisotropic behavior and processing requires specific powder sizes with correspondingly high prices. This study therefore addresses the feasibility of investment casting to produce open cellular structures. A high manganese X30Mn22 base alloy with different contents of aluminum (0, 1 and 5 wt %) was used for the manufacturing of a newly designed cell structure. Processing parameters and mold materials needed to be adjusted due to pronounced chemical reactions with the commercial SiO_2-based mold material. Using an Al_2O_3-based mold material and increasing the mold temperature during casting to 1000 °C allowed for the successful casting of high manganese steel structures with different designs regarding the strut diameter. Quasi-static compression tests of the structures confirm the cast quality and illustrate the effect of increasing alloying contents of Al on the deformation behavior, building the foundation for the development of programmable cellular structures for energy absorbing applications.

Keywords: open-cell metal structures; periodic open cellular structures; POCS; investment casting; high manganese steels; HMnS; lost form process; TRIP-effect; TWIP-effect

1. Introduction

High manganese steels (HMnS), also referred to as 2nd generation advanced high strength steels (AHSS), offer enhanced wear resistance, high toughness, and pronounced work-hardening during deformation which leads to their adoption in a variety of applications, including mining, railroad, defense, and automotive [1–5]. These steels typically contain 15 to 30 wt % of manganese to stabilize the austenitic phase. Depending on the stacking fault energy (SFE), secondary deformation mechanisms can be activated in addition to dislocation glide. In general, steels with a low SFE (typically below 15 mJm^{-2}) the main deformation mechanism is transformation-induced plasticity (TRIP) while HMnS with a medium SFE typically deform via twinning-induced plasticity (TWIP) and a high SFE allows for dislocation glide and shear banding [6]. For the activation of the TWIP mechanism in HMnS, different ranges of the SFE of 12–35 mJ/m^2 [7] 25–60 mJ/m^2 [8] and 25–80 mJ/m^2 [9] have been proposed. By alloying HMnS with aluminum, the SFE and the resulting microstructure and mechanical behavior can be varied in a wide range, as studied for an X30Mn21 base alloy [10], an X30Mn22 base alloy [11] and for Fe-16Mn-1.5C (wt %) steels [12]. For a low content of Al (about 1 wt %), the microstructure is still fully austenitic (fcc) and changes to a fcc-bcc duplex microstructure with increasing Al-content of up to 5 wt %. From 0 to 2 wt % Al the average grain size increased and decreased significantly with further increasing Al content (up to 5 wt %) [10]. Due to the good ductility and pronounced work-hardening of the alloy containing 5 wt % of aluminum, these HMnS are ideal candidates for use as structural components as well as energy-absorbing open cellular structures, making them suitable for various applications in automotive and aerospace.

Open cellular metal structures are often produced by investment casting, for example by using commercial open-cell polymer foams as a template [13–16]. Since their cell structure is stochastic, the properties cannot be predicted as reliably as with ordered structures [17,18]. The use of polymeric templates therefore significantly reduces the adaptability of the structure. In order to exploit the full potential, it is necessary to develop the structure according to its future purpose. Computer-aided design (CAD) can be employed to tailor (cellular) structures, which can then be used directly e.g., for additive manufacturing (AM). In this way, the structure can be adapted very well to the needs. Possible applications are demonstrated in [2]. Recent advancements in additive manufacturing have further enhanced the potential for designing complex, customized shapes of open cellular structures, broadening their applicability and performance in practical uses, including the design of programmable materials [19–21]. Previous studies have also demonstrated the potential of HMnS as a very promising material for the additive manufacturing of complex cellular structures [10,22,23]. However, AM generally requires powders with special grain size distributions which entails higher material costs, especially for larger quantities or overall increasing structure sizes. In this context, casting offers the potential for scalability and reduced costs for future industrial applications. Due to their layered construction, AM components usually exhibit anisotropic and heterogeneous microstructures that could be a disadvantage regarding mechanical properties in conventional practice engineering applications [10,11,24,25]. In addition, powder bed processes pose a significant health risk to operators due to skin contact or inhalation of the powder [26].

To date, research regarding the casting of HMnS is limited to ingot, and strip casting [27,28] as well as sand casting of bushes [29]. Mass production by continuous casting is impeded by severe chemical reactions of the Mn and Al with SiO_2 in conventionally used CaO-SiO_2-based mold fluxes [30–32]. The objective of this study is to combine the adjustable mechanical properties of HMnS resulting from the activation of multiple deformation mechanisms, *i.e.*, dislocation slip, TRIP and TWIP with the potential for lightweight design offered by open cellular structures by using an investment casting process. A periodic open-cellular structure (POCS) was designed, comprising a single unit cell that can be scaled in size and number to accommodate specific geometries according to the intended application. The aim is to combine a pronounced plateau stress in the compression stress-strain diagram at a high compressive stress level leading to a high energy absorption capacity. Experimental investment casting of the POCS was conducted with a 316 L steel and three HMnS containing different amounts of aluminum (X30Mn22, X30MnAl22-1 and X30MnAl22-5) based on the processing parameters evaluated in our previous study [33]. In these investigations a simplified geometry was employed, namely a step wedge with varying thicknesses, to delineate the boundaries and the impact of mold filling. In addition, it was found that the melt and the SiO_2-based mold material exhibited pronounced reactivity. Consequently, methods to circumvent these reactions were explored. The findings indicated that incorporating additional zirconium oxide layers could prevent the reactions. In addition, high-corundum mold materials were evaluated and initially posed an option for the successful casting. By further analysis of the mold material and optimizing the processing parameters, namely mold material composition and temperature during casting, POCS with different scales and strut diameters were successfully cast and characterized in this study. In further studies the results shall be compared to the results achieved with additively manufactured structures of the same design that are given in [11].

2. Design, materials and methods

2.1. Design of the periodic open cellular structure

Starting point of the POCS design was the face-centered cubic f2cc,z structure used in additive manufacturing [34–36] that is shown in Figure 1a. Under uniaxial stress this design activates a stretch dominated deformation mode that allows for a high tensile and compression strength as well as high specific energy absorption and is therefore very well suited for crash-relevant components [37]. In addition, the structure was successfully implemented for a HMnS with different amounts of aluminum [10]. However, since the bending direction of the vertical z-struts in this structure cannot be predicted for compressive load and may lead to pronounced strain localization [11,37], a different complex POCS was designed using the CAD software Catia (Dassault Systèmes, Vélizy-Villacoublay, France), see Figure 1c). This new structure comprises of straight diagonal struts and curved vertical struts, which (under compressive load) are bent to achieve a controlled deformation by compression in the z-direction as opposed to straight vertical struts and avoids buckling as shown for additively manufactured samples [11]. The radius of curvature (2.8 mm) for the vertical struts was selected as a compromise between pre-defining the direction of deformation and obtaining sufficient space for deformation without premature contact.

Although it was planned to compare the "ProZell" structure for both casting and additive manufacturing and this was taken into account in the design of the structure (no horizontal struts), the process-specific features first had to be considered and incorporated into the design of the structures. For casting, the minimum size of the structure is constrained by the printing process of the template, the stability of the template, and the post-processing regarding the removal of the mold material after casting. The maximum size is limited by the used casting device. For this study the initial structure design was with a unit cell size of 10 mm (“scale 2”) and later downscaled to 5 mm (“scale 1”), as shown in Figure 2 and Table 1. Furthermore, the strut diameter of the structure, and thus the relative density, was varied (see Figure 2) to investigate the influence of strut diameter on mechanical properties and deformation behavior. Furthermore, the feasibility limits of the casting process were to be tested. The tested variations are given in Table 1.

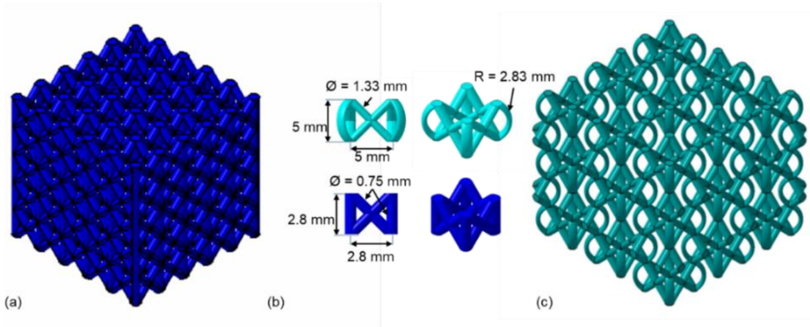

Figure 1. CAD designs of the f2cc,z structure (blue) [2] and the new “ProZell” structure (turquoise, Variation 1, scale 1).

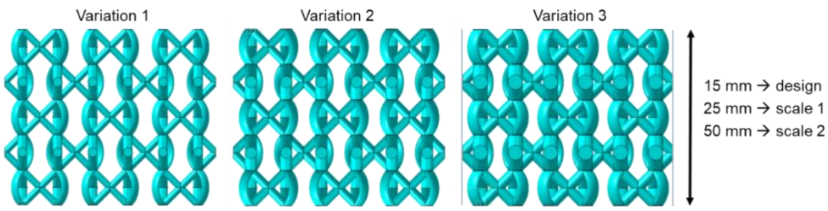

Figure 2. Newly designed POCS “ProZell” with different strut diameters: 0.8/1/1.25 mm (left to right).

Table 1. Structure and definition of the variations scaled for casting.

Cell design	Scale	Unit cell size [mm]	Strut ø [mm]	Porosity [%]
Variation 1	2	10	2.67	87.6
Variation 1	1	5	1.33	87.6
Variation 2	1	5	1.66	81.3
Variation 3	1	5	2.09	72.4

2.2. Materials

The metals used for the casting experiments were a 316 L austenitic stainless steel (X2CrNiMo17-12-2) and three HMnS with different amounts of aluminum, *i.e.*, 0%, 1% and 5%, respectively. The chemical compositions are given in Table 2.

Table 2. Chemical compositions (in wt %) of used casting materials 316 L (X2CrNiMo17-12-2) and HMnS with different amounts of aluminum.

	C [%]	Si [%]	Mn [%]	Al [%]	Cr [%]	Mo [%]	Ni [%]	Fe [%]
X2CrNiMo17-12-2	≤ 0.03	≤ 1.0	≤ 2.0	-	16.5–18.5	2.0–2.5	10.0–13.0	balance
X30Mn22	0.29	0.03	22.10	0.004	0.09	0.03	0.01	balance
X30MnAl22-1	0.28	0.2	22.60	0.93	0.09	0.04	0.01	balance
X30MnAl22-5	0.31	0.01	22.80	5	0.09	0.04	0.01	balance

Different mold materials were tested for their feasibility in the casting process of HMnS. These include the standard SiO_2-based mold materials ProHT Steel and ProHT Platinum (Goodwin Refractory Services, Newcastle-under-Lyme, UK) as well as two high-corundum mold materials, namely Carath 1804 (RATH AG, Vienna, Austria) and Keroxyd (OXYD-KERAMIK GmbH & Co. KG, Lügde-Elbrinxen, Germany), with their chemical composition given in Table 3. Since previous experiments indicated very strong chemical reactions between the SiO_2-based mold material ProHT and the HMnS (see also [33]), additional zirconium-based layers were applied for selected castings of the POCS. For this, the initial wax models were immersed in a zirconium oxide slurry (Ransom & Randolph GmbH, Rötha, Germany) to apply a layer with a thickness of approximately 0.5 mm and subsequently sprinkled with zirconia sand. This was conducted twice to have two layers. To fully dry the coating layer the model was dried for at least 2 hours at room temperature.

The Al_2O_3-based molding materials showed no strong reactions with the liquid HMnS in our earlier study [33]. However, the high hardness of these molding materials proved to be a disadvantage, as the burnt mold material could only be removed to a limited extent from the cast cellular structures. To resolve this issue, the standard Keroxyd casting compound was adjusted by the manufacturer by adding cellulose (< 0.1%) and a hydrocolloid (< 0.05%). This modified Keroxyd was then prepared with an increased amount of water and burnt at relatively low temperatures.

Table 3. Chemical composition (in wt %) of the used mold materials Carath and Keroxyd (manufacturer's specification).

	Al_2O_3 [%]	SiO_2 [%]	CaO [%]	MgO [%]	Fe_2O_3 [%]	Na_2O [%]
Carath 1804 ULC	97.8	0.15	1.5	-	0.15	-
Keroxyd	96.5	< 0.2	2.7	0.1	< 0.1	0.2

2.3. Casting process

In this study, the investment casting was conducted with a printed wax template. Opposed to other investment casting processes, no shell application (as described e.g. in [38]) was used because the designed structures are so fine that there is not enough space in the inner part to build a shell. The processing steps are shown in Figure 3. In the initial stage (a), the wax template is printed with a ProJet MJP 2500W 3D printer (3D Systems, Moerfelden-Walldorf, Germany). Additional support wax (white) is used to stabilize the structure wax (violet) during printing. The support wax is then removed from the template in a stirred and heated isopropanol bath, providing the open cellular preform (b). For the casting process, a feeder is added to the base plate of the wax model. A cuvette is then placed upon the plate and sealed by wax (c). Using a KWS Investment Mixing Machine the mold material is mixed according to the manufacturer's instructions and filled into the cuvette (d, e). Depending on the used mold material, the drying phase is followed by a burning, where the wax is also melted out. The steel (from premade ingots) is molten and cast in a VC 480 V vacuum pressure casting machine (Blue Power Induction, Amityville, NY, USA) with a casting temperature of 1,580 °C (f). Once the casting temperature has been reached, pre-heated cuvettes (850 °C) are transferred from an oven to the casting device, and the mold is filled with molten metal. For casting the pressure was set to 1.5 bar and the flask pressure was −1 bar. After solidification and cooling, the mold material is removed using high-pressure waterjet and sandblasting techniques (g). Finally, the samples are detached from the base plate by sawing or wire eroding.

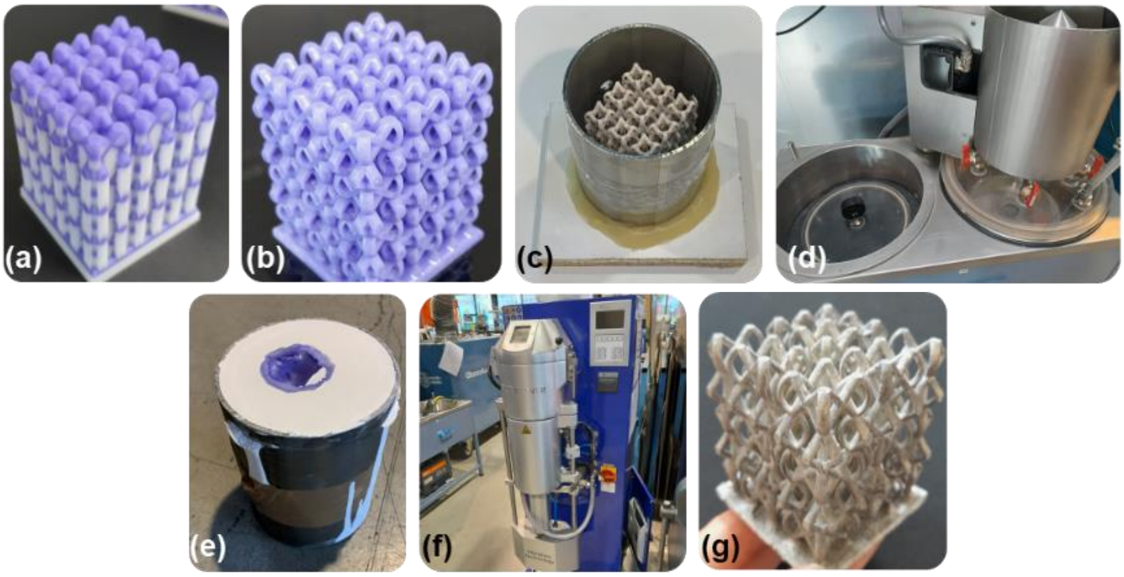

Figure 3. Process route from 3D printed model (a) to cast part (g).

2.4. Methods for characterization

X-ray diffraction (XRD) was used for quantitative analysis of mold reactions on cast step wedges [33]. XRD patterns were collected in a Bruker D8 DISCOVER (Bruker Corporation, Billerica, MA, U.S.A.) using Co-Kα-radiation. The patterns were recorded in the 2θ angular range of 20°–130°. The 2θ angular steps were 0.3°. For evaluation, the background was subtracted, the $K\alpha_2$ radiation was subtracted and the diffractogram was smoothed.

For characterization of the mold materials 3-point bending tests were performed with a support distance of 60 mm as shown in Figure 4. The radii of the bending punch and the supports were 5 mm. Bending bars with dimensions of 23 × 20 mm² were produced from the SiO_2- (ProHT Steel and ProHT Platinum) and Al_2O_3-based (Carath 1804 ULC, Keroxyd, modified Keroxyd) molding materials prepared according to the manufacturer's specifications.

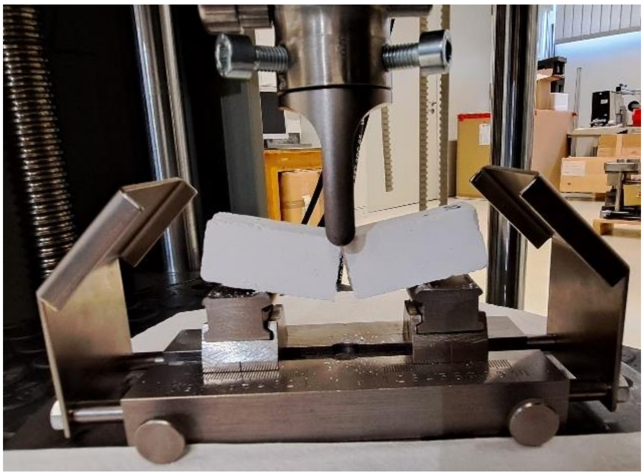

Figure 4. Photograph of the 3-point bending test setup (supports distance: 60 mm. Bending punch and support: R = 5 mm).

Compression tests were performed at room temperature on POCS specimens based on DIN 50134 using a servo-hydraulic universal testing machine (Carl Schenck AG, Darmstadt, Germany) equipped with a 1000 kN load cell at a constant strain rate of 0.001 s^{-1}. The displacements were recorded with a linear variable differential transformer. Due to the high effort required for sample production only two samples per combination of Al content and structure variant were tested.

3. Results

3.1. Evaluation of the mold material

The results of the 3-point bending tests are given in Table 4. In most cases, the bars broke immediately after the load was applied without a significant drop in force. In many samples, the force drops and deflection at break were so low that the testing machine did not detect a break signal and therefore no precise figure for the breaking force was determined. The samples disintegrated when the punch was retracted. Therefore, only the maximum forces were used for the evaluation. The bending bars of the ProHT Platinum and ProHT Steel exhibited the lowest maximum forces. This was followed by the bending strength of the mold materials modified Keroxyd, pure Keroxyd and Carath 1804. Though the mean value of the maximum force was significantly lower for the modified Keroxyd, a clear differentiation of the bending strengths of the two Keroxyd mold materials was challenging due to the sparse database and the widely scattered data that may result from defects like larger pores in the bending bars.

These results offer a first quantitative indication for the feasibility of the different mold materials. A qualitative evaluation confirmed that a low strength of the mold material is favorable for the wash-out behavior. Based on these findings the SiO_2- and Al_2O_3-based mold material with the lowest bending strength were chosen for the casting experiments, *i.e.*, ProHT Steel and modified Keroxyd.

Table 4. Results of the bending tests (F_m–maximum force).

Base	Mold material	$F_{m,1}$ [N]	$F_{m,2}$ [N]	$F_{m,3}$ [N]	$F_{m,4}$ [N]	$F_{m,5}$ [N]	$F_{m,\ mean}$ [N]	$F_{m,\ sd}$ [N]
SiO_2	ProHT Platin	9.5	11.0	13.8	11.6		11.5	1.5
SiO_2	ProHT Steel	0.90	2.80	2.70			2.1	0.9
Al_2O_3	Carath 1804	252.9	132.0	599.7	685.4		417.5	231.1
Al_2O_3	Keroxyd pure	37.6	249.5	110.6	86.6		121.1	78.7
Al_2O_3	Keroxyd modified	142.5	77.3	138.9	93.6	86.6	107.8	30.6

As described in detail in our earlier study [33] casting of HMnS in the ProHT mold material resulted in the formation of an unfavorable surface, a lack of geometric precision and an unclean separating surface. These factors collectively impeded the unpacking process.

It was assumed that the molten HMnS reacted with the SiO_2 of the ProHT mold material, as observed for casting of HMnS with high Al content using $CaO–Al_2O_3–SiO_2$ based mold fluxes [31,32]. To validate this, a quantitative phase analysis was performed on a X30Mn22 sample cast under inert gas (argon) atmosphere in a ProHT steel mold heated to 700 °C.

The first measurement was conducted on the scale layer of the sample (Figure 5, left). The phase analysis identified ferrite and martensite as the main phases. Iron oxides such as magnetite (Fe_3O_4), hematite (Fe_2O_3), wustite (FeO) and $Mn_{0,43}Fe_{2,57}O_4$ were also detected. The analysis also suggests that a FeO-MnO and a Fe-Mn solid solution are present in the layer. The analyzed layer also contained SiO_2

in the form of cristobalite and quartz. Since the melting and casting took place in an argon atmosphere, it is likely that the oxides were formed due to reactions between the HMnS and the mold material.

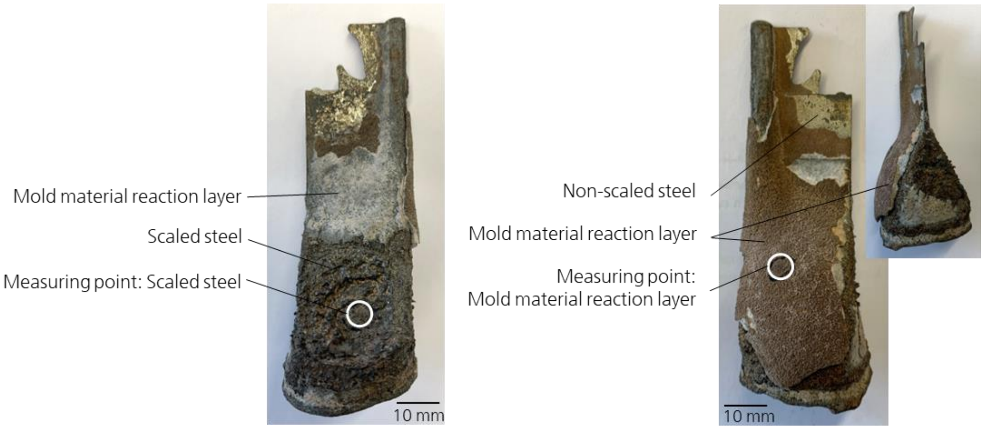

Figure 5. Cast step wedge, with areas of strong surface deformation (left) and mold reaction (right).

The second measurement was conducted on the layer of the reaction area (Figure 5, right). In addition to SiO_2 in the form of cristobalite and quartz, which originate in the molding material, a monocline $Mg_2Mn(PO_4)$ phase was identified. X-ray fluorescence analysis confirmed the presence of manganese, phosphor, and magnesium. It is evident that the manganese is derived from the steel, while phosphor, oxygen, and magnesium are transferred from the mold material.

In order to prevent these adverse reactions, additional zirconium layers were applied to the 3D printed pre-forms before casting in ProHT Steel molds, as proposed in [33].

3.2. Experimental casting

For the first trial castings of the POCS the structure variant 1 with a scale of 2 was selected. ProHT Steel was used for the mold. This approach proved to be more conducive to the handling of the wax pattern, unpacking, and evaluation of the mold filling and surface quality. Initially, castings were conducted with 316 L (no additional zirconium layer) to generally assess mold filling without the influence of metal-mold reactions.

A highly accurate reproduction of the structure was achieved without any adverse reactions, resulting in a high-quality surface finish. However, upon embedding the structure into the molding material, small air bubbles became trapped, which were then reproduced in the casting. This process was then successfully adapted by applying a vacuum pressure of −1 bar during embedding to prevent bubbles from being included.

In one out of four cast structures, two missing connections of the struts were observed due to cold runs. The other three structures were successfully reproduced. Unpacking of the structures was a time-consuming process as the inner structure is hardly accessible by mechanical cleaning and the mold material turned out to be very hard despite its low bending strength.

By adding two supplementary zirconium layers, no significant reactions with the mold material were observed. However, the zirconium oxide layer cracked, particularly in the region near the feeder, which resulted in a replication of the cracks in the cast part (Figure 6a). Nevertheless, a very good reproduction of the structure with only a few cold runs was achieved.

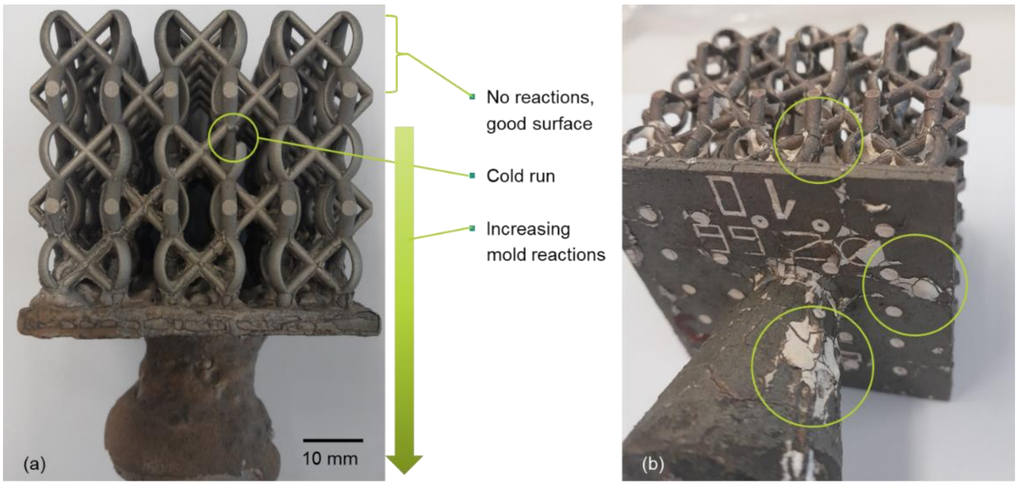

Figure 6. Photographs of cast samples. **(a)** X30Mn22, sandblasted, with good geometry reproduction and increasing reactions towards the feeder; **(b)** 316L with residues of the zirconium oxide layer (bright areas) and marked replicated cracks (circles).

For castings of X30Mn22 under equal conditions (V1S2, ProHT Steel) similar results can be observed, though the additional zirconium oxide layers prevented the adverse chemical reactions to a large extent. It was observed that there were no reactions and thus a good surface quality was achieved at the bottom of the structure, *i.e.*, opposite the feeder. Towards the feeder, pronounced reactions occurred, as illustrated in (Figure 6a). A few cold runs were also observed. Based on previous experiments with zirconium layers, it was hypothesized that the interval between the deposition of the layer and the molding process can influence the stability of the layers, but no significant differences were identified for different dwell times of 0.5 h, 3 h, or 2 days. It is more likely that the very high temperatures during casting are causing the zirconium oxide layer to be unstable and causing cracks, preventing a good reproduction of the structure regardless of the melt material.

The use of modified Keroxyd as the mold material for X30Mn22 casting (V1S2) resulted in the production of a highly accurate reproduction of the structure, free from any adverse reactions. Some samples exhibited a few instances of cold runs (Figure 7**,** left and middle), while others did not. Compared to the ProHT Steel mold material, the process of removing the mold material from the structure was more time-consuming.

For castings of POCS with a scale of 1, the mold material proved to be particularly difficult to remove due to the small dimensions of 30 × 30 × 25 mm^3. The reproduction of the structure was in general highly accurate, yet only about 80% of the structure were filled due to rapid solidification of the melt. To prolong the material flow and ensure a complete filling of the structure the mold temperature was increased to the machine maximum of 1000 °C. Although the preliminary investigations on the step wedge [33] indicated that increasing the mold temperature to 1000 °C did not result in improved filling degree, the outcome for the POCS was favorable. The structures were reproduced very well, exhibiting a high-quality surface and no evidence of cold runs (Figure 7, right). Applying negative pressure during the mold-making process was successful in preventing bubbles from forming, which could otherwise be reproduced in the structure during casting.

Figure 7. Left, middle: cold runs; right: sample with sandblasted surface in scale 1, variation 1.

This set of parameters was then employed to manufacture samples with different combinations of strut diameters (variation 1–3, scale 1) and alloys (X30Mn22, X30MnAl22-1, X30MnAl22-5) as detailed in Figure 8. The casting results were, for the most part, satisfactory.

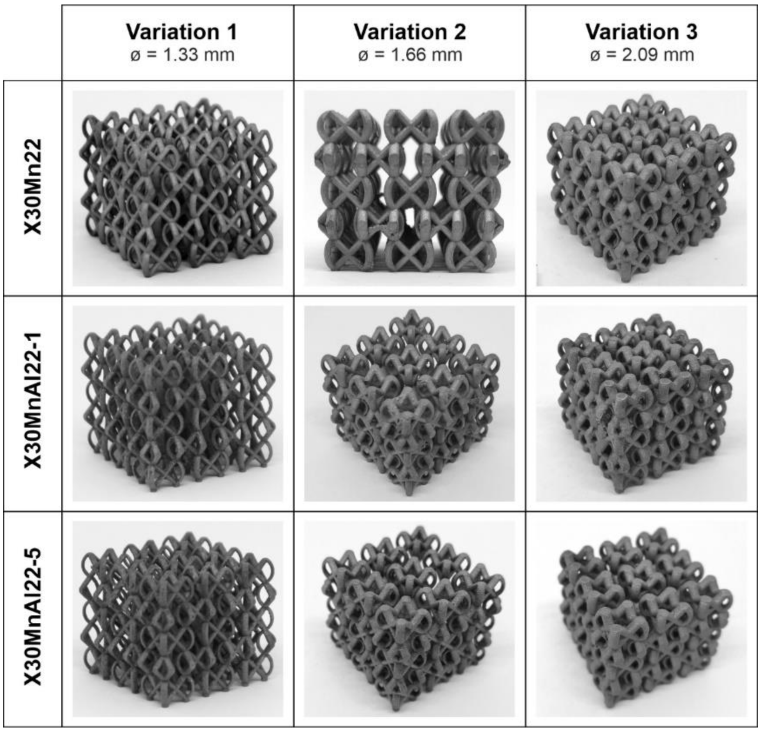

Figure 8. Overview of cast structures (scale 1; size: 30 × 30 × 25 mm²).

However, the molds did occasionally crack slightly during the burning cycle, which resulted in a lack of precise replication of the geometry and the presence of casting flashes (see Figure 9). These could be removed subsequently in most cases.

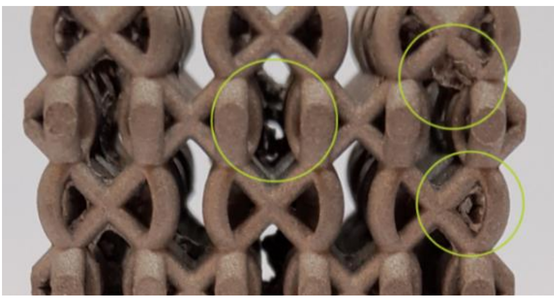

Figure 9. Variation 3 sample made in a slightly cracked mold with casting defects (flashes).

3.3. Characterization of cast structures

The successfully cast POCS were tested in quasi-static compression tests. Figure 10 shows a sequence of photographs taken during the test of a V1S2 sample at different levels of compression. The deformation behavior of the designed POCS can be easily observed due to the small strut diameter. In comparison to the f2cc,z structure (see [22,37]), where the z-struts bend in random directions and therefore the deformation behavior is not predictable, the "ProZell" structure in principle deforms as initially intended by the design. The curved struts bend and with higher force the struts forming an x deform in a way that is comparable to a scissor lift (Figure 11) in a very homogenous way. In comparison to the f2cc,z structure [37,39] no collective failure occurred.

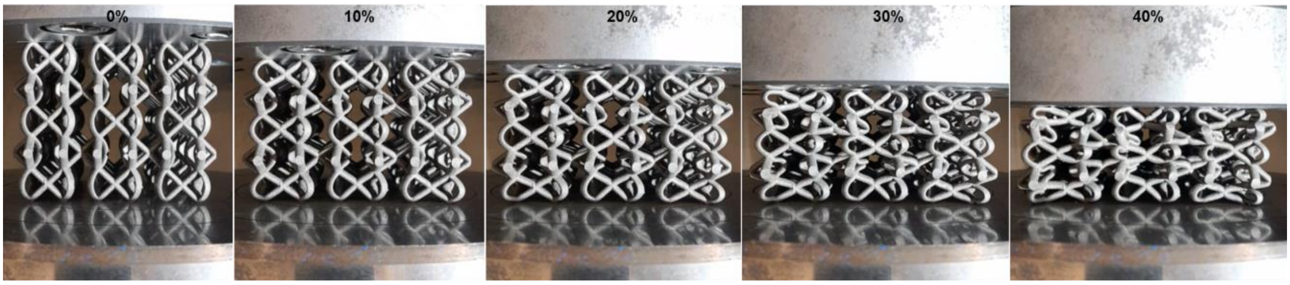

Figure 10. Compression test of a cast sample (V1) at different levels of compression (0%–40%).

Figure 11. Detail of undeformed structure (V1, scale 2) and deformed under compressive load. Right: example for random bending of z-struts under compression load [37].

Results of the compression tests for cast POCS with a scale of 1 are given in Figure 12 (left) for different contents of Al and structure variants 2 and 3. Since the forces required for the deformation of the variant 1 (smallest strut diameter) are comparatively low, only the results for the variants 2 and 3 are compared in the following.

In general, a pronounced plateau of compressive force was observed, which was the objective parameter of the structure design. The reproducibility of the results is very good, even with only two samples per combination. It can be seen that the compressive force was higher in the V3 samples compared to V2 specimens, due to the increased strut diameter, which was also reflected in the weight-specific energy absorption (SEA) values until 40% deformation per total mass of the sample, Figure 12. The compressive force continued to increase in V3 samples until densification, whereas it followed more of a plateau-like trend in V2 samples.

For both POCS variants V2 and V3, the samples cast with Al0 showed the highest degree of work hardening, which results from a pronounced TRIP effect as shown for POCS with a f2cc,z unit cell manufactured by AM by Köhnen *et al.* [10]. With increasing amount of aluminum and therefore increasing SFE, they reported a shift of the deformation mechanism from TRIP to a combination of TRIP/TWIP and finally a dominant TWIP effect for an aluminum content of 5 wt %. The cast Al1 samples did not follow the same trend. This may be related to the inability to effectively activate the twinning in the cast Al1 samples. In this case, the overall strength of the cast Al5 samples could be higher than that of the cast Al1 samples due to finer grains in the duplex (fcc-bcc) microstructure and efficient solution hardening by higher Al. However, detailed microstructure analysis is required for a deeper understanding of the underlying mechanisms, which was beyond the scope of this study. Correspondingly, the degree of work hardening of the AM open cellular structures decreased even for small additions of Al (Al1) while the yield force increased significantly only for higher additions of Al (Al5). Similar results can be found for the cast POCS of variant V3 (Figure 8). For the V2 samples, a decrease in work-hardening for samples of Al1 and Al5 was also found but due to the overall lower yield forces no significant increase in yield force was detected for Al5. However, it can in general be concluded that POCS of HMnS can be cast successfully with the processing parameters elaborated in this study and the deformation behavior of the cast HMnS structures is in general comparable to AM structures that were studied in [11]. The weight-specific energy absorption for Al0_V2 is 7.9 J/g for additively manufactured samples in comparison to 8.6 J/g for cast samples (see Figure 12 and for Al0_V3 it is 12.8 J/g *versus* 13.6 J/g, respectively.

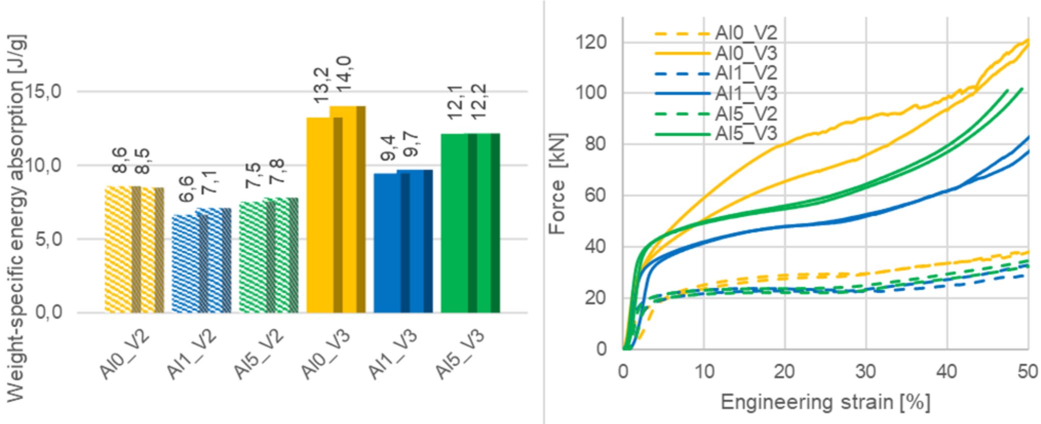

Figure 12. SEA-values until 40% strain (left) and representative compressive force-engineering strain curves of cast samples with different contents of Al for of POCS variants 2 and 3 (V2, V3).

Finally, the SEA values indicate that the changes in energy absorption capacity are mostly related to sample geometry (increasing SEA with increasing strut diameter).

4. Summary and conclusion

In this study we evaluated the feasibility of the investment casting process to produce fine and complex open cellular structures using HMnS with different amounts of aluminum. By adapting the mold material and preparation routine as well as the mold temperature during the casting process high-quality surfaces and accurate replications of the structure in different scaling and with different strut diameters could be realized. The best results were achieved by using modified Keroxyd for the mold and casting with a melt temperature of 1580 °C and a mold temperature of 1000 °C. Characterization of the cast structures by compression tests confirmed that the POCS' in general deform as intended by the new "ProZell" structure design. The weight specific energy-absorption values for the AL0_V2 variation, is 8.6 J/g; for the Al1_V2 variation, it is 6.9 J/g; and for the AL5_V2 variation, it is 7.7 J/g. The SEA values achieved up to 40% strain for structures with thicker struts (V3) are significantly higher than for structures with thinner struts (V2). The values achieved are 13.6 J/g for Al0_V3, 9.6 J/g for Al1_V3 and 12.2 J/g for Al5_V3. For the structures with the smaller strut diameter of 1.66 mm (V2) a pronounced plateau of the force during compression is achieved. Since achieving stable and predictable deformation is a key goal for crash absorbers [40], the structure can be used as a good base for such applications. Between 13% and 30% of engineering strain the force is very stable at around 22 kN (V1 Al0 and Al5).

Further research is needed to improve the process and mold material to reliably prevent cracking in the mold and to achieve easier removal of fine and complex samples. The modified Keroxyd shows a high potential to achieve this goal, but there are still unknown influences on the mold material behavior, given that molds made from the same compound can exhibit significantly different properties after casting, as assessed in the 3-point bending tests.

The presented procedure and successful POCS castings constitute the starting point for further microstructural and mechanical investigations. In this context, the focus is on the influence of the aluminum content on the casting microstructure and the resulting local deformation mechanisms in terms of TRIP and/or TWIP effects. The final aim is to compare the cast POCS with additively manufactured samples.

Data availability statement

The data that support the findings of this study are available from the corresponding author upon reasonable request.

Acknowledgments

The authors gratefully acknowledge funding by the German Research Foundation (Deutsche Forschungsgemeinschaft, DFG) in project “ProZell” (project ID 437986279). The authors thank OXYD-KERAMIK GmbH & Co. KG for supporting us with the mold material.

Authors’ contribution

Conceptualization, Christian Haase, Jörg Hohlfeld, Ulrich Krupp; methodology, Claudia Drebenstedt, Nadja Berndt; formal analysis, Claudia Drebenstedt, Dilay Kibaroglu, Nadja Berndt; investigation, Jörg Hohlfeld, Christian Hannemann, Claudia Drebenstedt; resources, Ulrich Krupp, Thomas Hipke; writing—original draft preparation, Nadja Berndt, Claudia Drebenstedt; writing—review and editing, Claudia Drebenstedt, Jörg Hohlfeld, Christian Hannemann, Nadja Berndt, Ulrich Krupp, Thomas Hipke, Dilay Kibaroglu, Christian Haase; visualization, Claudia Drebenstedt, Jörg Hohlfeld; project administration, Ulrich Krupp, Jörg Hohlfeld; funding acquisition, Thomas Hipke, Ulrich Krupp, Christian Haase, Jörg Hohlfeld. All authors have read and agreed to the published version of the manuscript.

Conflicts of interests

The authors declare that they have no known competing financial interests or personal relationships that could have appeared to influence the work reported in this paper.

References

[1] World Foundry Organization. In 71st World Foundry Congress: Advanced Sustainable Foundry, WFC 2014, Bilbao, Spain, May 19–21, 2014.

[2] De Cooman BC, Chin K, Kim J. High Mn TWIP steels for automotive applications. In New Trends and Developments in Automotive System Engineering. London: IntechOpen, 2011.

[3] Cheng B, Wei F, Teh WH, Cheong KH, Lee JJ, *et al*. High strength Hadfield steel produced using laser powder bed fusion of mixed powders. Mater. Des. 2023, 231:112017.

[4] Scheller P, Weiss A. High-manganese steel alloy. WO Patent No. 2006/125412 A1, 30 Nov. 2006.

[5] Bouaziz O, Allain S, Scott CP, Cugy P, Barbier D. High manganese austenitic twinning induced plasticity steels: A review of the microstructure–properties relationships. Curr. Opin. Solid State Mater. Sci. 2011, 15(4):141–168.

[6] De Cooman BC, Estrin Y, Kim SK. Twinning-induced plasticity (TWIP) steels. Acta Mater. 2018, 142:283–362.

[7] Allain S, Chateau J P, Bouaziz O, Migot S, Guelton N. Correlations between the calculated stacking fault energy and the plasticity mechanisms in Fe–Mn–C alloys. Mater. Sci. Eng., A 2004, 387:158–162.

[8] Remy L, Pineau A. Twinning and strain-induced fcc → hcp transformation on the mechanical properties of Co Ni Cr Mo alloys. *Mater. Sci. Eng.* 1976, 26(1):123–132.

[9] Remy L, Pineau A. Twinning and strain-induced FCC → HCP transformation in the Fe Mn Cr C system. *Mater. Sci. Eng.* 1977, 28(1):99–107.

[10] Köhnen P, Ewald S, Schleifenbaum JH, Belyakov A, Haase C. Controlling microstructure and mechanical properties of additively manufactured high-strength steels by tailored solidification. *Addit. Manuf.* 2020, 35:101389.

[11] Kibaroglu D, Katti A, Drebenstedt C, Hipke T, Krupp U, *et al.* Enhancing energy absorption performance in additively manufactured lattice structures: A synergistic approach to geometry and alloy design. *Mater. Des.* 2025, 254:114021.

[12] Tang Y, Li B, Zhang G, Ji P, Zhang X, *et al*. Effect of Al on the microstructure and corrosion resistance of high-Mn steel. *Mater. Lett.* 2022, 320:132286.

[13] Kulshreshtha A, Dhakad S K. Preparation of metal foam by different methods: a review. *Mater. Today Proc.* 2020, 26:1784–1790.

[14] Li JP, Li SH, Van Blitterswijk CA, de Groot K. A novel porous Ti6Al4V: characterization and cell attachment. *J. Biomed. Mater. Res. Part A* 2005, 73(2):223–233.

[15] Bakan HI, Korkmaz K. Synthesis and properties of metal matrix composite foams based on austenitic stainless steels–titanium carbonitrides. *Mater. Des.* 2015, 83:154–158.

[16] Frömert J, Lott TG, Matz AM, Jost N. Investment casting and mechanical properties of open-cell steel foams. *Adv. Eng. Mater.* 2019, 21(6):1900396.

[17] Lehmhus D, Vesenjak M, De Schampheleire S, Fiedler T. From stochastic foam to designed structure: balancing cost and performance of cellular metals. *Materials* 2017, 10(8):922.

[18] Novak N, Al-Ketan O, Mauko A, Yilmaz YE, Krstulović-Opara L, *et al*. Impact loading of additively manufactured metallic stochastic sheet-based cellular material. *Int. J. Impact Eng.* 2023, 174:104527.

[19] Degischer HP, Krisz B. *Handbook of Cellular Metals: Production, Processing, Applications.* Weinheim: Wiley-VCH, 2002.

[20] Yang L, Wiener S, Medina F, Menon M, Baughman B. *Additive Manufacturing of Metals: The Technology, Materials, Design and Production*. Cham: Springer, 2017.

[21] Do G, Geißelbrecht M, Schwieger W, Freund H. Additive manufacturing of interpenetrating periodic open cellular structures (interPOCS) with in operando adjustable flow characteristics. *Chem. Eng. Process. Process Intensif.* 2020, 148:107786.

[22] Kies F, Köhnen P, Wilms MB, Brasche F, Pradeep KG, *et al*. Design of high-manganese steels for additive manufacturing applications with energy-absorption functionality. *Mater. Des.* 2018, 160:1250–1264.

[23] Haase C, Bültmann J, Hof J, Ziegler S, Bremen S, *et al*. Exploiting process-related advantages of selective laser melting for the production of high-manganese steel. *Materials* 2017, 10(1):56.

[24] Kok Y, Tan XP, Wang P, Nai MLS, Loh NH, *et al*. Anisotropy and heterogeneity of microstructure and mechanical properties in metal additive manufacturing: a critical review. *Mater. Des.* 2018, 139:565–586.

[25] Huangfu B, Liu Y, Liu X, Wu X, Bai H. Anisotropy of additively manufactured metallic materials. *Materials* 2024, 17(15):3653.

[26] Chen R, Yin H, Cole IS, Shen S, Zhou X, *et al*. Exposure, assessment and health hazards of particulate matter in metal additive manufacturing: a review. *Chemosphere* 2020, 259:127452.

[27] Daamen M, Wietbrock B, Richter S, Hirt G. Strip casting of a high-manganese steel (FeMn22C0.6) compared with a process chain consisting of ingot casting and hot forming. *Steel Res. Int.* 2011, 82(1):70–75.

[28] Daamen M, Richter S, Hirt G. Microstructure analysis of high-manganese TWIP steels produced via strip casting. *Key Eng. Mater.* 2013, 554–557:553–561.

[29] Alrobei H, Malik RA, Amjad F, AlBaijan I. Investigation of structure and mechanical characteristics of a high manganese steel via SolidCast simulation method. *Metals* 2023, 13(3):572.

[30] Ou G, Liu Y, Yen S, Wang H, Su YH, *et al*. Reactivity and thermo-physical properties of MnO-modified CaO-Al2O3-based mold fluxes for advanced high-strength steels. *J. Mater. Res. Technol.* 2020, 9(6):12091–12101.

[31] Zhang J, Ai X, Guan R. Multicomponent reaction mechanism at steel-slag interface during continuous casting of high mn–al steels: modeling and experimental validation. *Metall. Mater. Trans. B* 2025.

[32] Wang Q, Zhang J, Ostrovski O, Zhang C, Cai D. Effect of Al2O3/SiO2 ratio on structure and properties of mold flux for high-al steel continuous casting. *J. Sustain. Metall.* 2025;11(2):877–887.

[33] Drebenstedt C, Hannemann C, Hohlfeld J, Siebeck S, Hipke T, *et al*. Custom design to the application of open-cellular metal structures. In *12th International Conference on Porous Metals and Metallic Foams 2024*, Dresden, Germany, July 5–7, 2023, pp. 25–31.

[34] Zhou X, Qu C, Luo Y, Heise R, Bao G. Compression behavior and impact energy absorption characteristics of 3d printed polymer lattices and their hybrid sandwich structures. *J. Mater. Eng. Perform.* 2021;30(12):8763–8770.

[35] Burkhardt C, Henkel S, Biermann H, Weidner A. Influence of alloy composition on microstructural and mechanical properties of lattice structures made of high-alloyed austenitic TRIP/TWIP steel produced by selective electron beam melting. *Mater. Sci. Eng., A* 2025, 930:148073.

[36] Rehme O. Cellular design for laser freeform fabrication. Doctoral Thesis, Hamburg University of Technology, 2009.

[37] Köhnen P, Haase C, Bültmann J, Ziegler S, Schleifenbaum JH, *et al*. Mechanical properties and deformation behavior of additively manufactured lattice structures of stainless steel. *Mater. Des.* 2018, 145:205–217.

[38] Pattnaik S, Karunakar DB, Jha PK. Developments in investment casting process—a review. *J. Mater. Process. Technol.* 2012, 212(11):2332–2348.

[39] Kotzem D, Arold T, Bleicher K, Raveendran R, Niendorf T, *et al*. Ti6Al4V lattice structures manufactured by electron beam powder bed fusion—microstructural and mechanical characterization based on advanced in situ techniques. *J. Mater. Res. Technol.* 2023, 22:2111–2130.

[40] Xu B, Wang C, Wang S. Crushing behaviours and energy absorption characteristics of square antiprisms structure against flatwise crushing. *Int. J. Impact Eng.* 2023, 172:104398.